Simulation of intravalley acoustic phonon scattering in silicon nanowires

Martin Frey, Aniello Esposito and Andreas Schenk
IIS Integrated System Laboratory
ETH Swiss Federal Institute of Technology
CH-8092 Zurich
Email: mfrey@iis.ee.ethz.ch

***Abstract*— In this paper, the influence of intravalley acoustic phonon scattering on transport through silicon nanowires is studied. The focus lies on a comparison of the full problem with approximate methods regarding the self-consistent electrostatics and current computation. In addition, the scaling behavior with increasing device lengths is shown.**

I. Introduction

In order to capture the physical effects relevant at the nanoscale, into which the size of metal-oxide-semiconductor field effect transistors (MOSFET) have entered, electronic transport through these devices should be described at the level of quantum mechanics (QM). The nonequilibrium Green's function (NEGF) formalism provides a framework, which allows to include different scattering mechanisms, such as electron-phonon scattering or impurity scattering on a perturbative approach. Since both electrons and phonons are described by wave functions, scattering in QM is a spatially correlated phenomenon. However, in order to decrease the computational burden, approximations can be made, such that scattering becomes local in space, see Section II-C.

In this work, we analyze the influence of intravalley acoustic phonon scattering on transport through silicon nanowires using deformation potential theory and the self-consistent Born approximation. A brief overview about the simulation procedure in the simulator *SIMNAD* is given in Section III. The results are compared with results from simulations that neglect renormalization effects of scattering [7] [8] and with ballistic simulations.

II. Quantum transport equation

A. Steady-state transport equations

In the NEGF formalism, the steady-state transport equations for the retarded (G^R) and the lesser ($G^<$) Green's function [1][2] are

$$\int dr_1[(E-H(r))\delta(r-r_1)-\Sigma^R(r,r_1)]G^R(r_1,r')=\delta(r-r') \tag{1}$$

$$G^<(r,r')=\int dr_1\int dr_2 G^R(r,r_1)\Sigma^<(r_1,r_2)G^A(r_1,r'), \tag{2}$$

where $H(r)$ is the Hamiltonian of the system and $\Sigma(r,r')$ the self-energy, containing all the interactions $\Sigma_{int}(r,r')$ (except the Hartree potential) as well as the boundary conditions $\Sigma_{bc}(r,r')$:

$$\Sigma(r,r')=\Sigma_{int}(r,r')+\Sigma_{bc}(r,r'). \tag{3}$$

B. Coupled mode expansion

The starting point for solving the quantum transport equations is the choice of a basis function set, in which all operators are expanded. In this work, we consider a parabolic bandstructure for silicon and express the effective mass Hamiltonian in the so-called coupled mode expansion. It has been shown that for devices with a simple geometry, i.e. devices with a well-defined transport direction, the coupled mode approach yields the same results as a real-space approach, yet decreasing the computational burden significantly [6].

In the coupled mode approach, the solution of the 3D Schrödinger equation is written as the product

$$\phi_n(r)=\varphi(x-x_i)\tilde{\phi}_n(x_i,y,z), \tag{4}$$

where $\varphi(x-x_i)$ is a function localized around a layer $x=x_i$ and the mode $\tilde{\phi}_n(x_i,y,z)$ is the solution of the transverse Schrödinger equation on the same layer:

$$H_\perp(x_i,y,z)\tilde{\phi}_n(x_i,y,z)=E_n(x_i)\tilde{\phi}_n(x_i,y,z) \tag{5}$$

with the transverse Hamiltonian defined as

$$H_\perp(x_i,y,z)=-\frac{\hbar^2}{2}\frac{\partial}{\partial y}(\frac{1}{m_y}\frac{\partial}{\partial y})-\frac{\hbar^2}{2}\frac{\partial}{\partial z}(\frac{1}{m_z}\frac{\partial}{\partial z})+V(x_i,y,z). \tag{6}$$

The Green's functions can now be expressed in the basis functions $\phi_n(r)$, i.e. for $G^R(r,r')$:

$$G^R(r,r')=\sum_{n,m}G^R_{nm}\phi^*_n(r)\phi_m(r'), \tag{7}$$

where G^R_{nm} is the solution of

$$\sum_{n'}\left(E\delta_{nn'}-\int dr\phi^*_n(r)H(r)\phi_{n'}(r)-\int dr\int dr'\phi^*_n(r)\Sigma^R(r,r')\phi_{n'}(r')\right)G^R_{n'm}=\sum_{n'}(E\delta_{nn'}-H_{nn'}-\Sigma^R_{nn'})G^R_{n'm}=\delta_{nm}. \tag{8}$$

Equation (8) is obtained by inserting (7) into (1), multiplying with $\phi^*_n(r)$ from the left and $\phi_{n'}(r')$ from the right and finally

integrate over r and r'.
The boundary self-energies are not transformed but directly computed in mode-space [4].
The advantage of the coupled mode approach lies in the reduction of the matrix size for the transport problem, since the square of the number of modes N_M^2 needed in the simulations is much smaller than the number of grid points (N_y, N_z) in the transverse direction: $N_M^2 \ll N_y \cdot N_z$.
On the other hand, one of the major shortcomings of this approach is that only transport along crystall direction (100) is possible for nanowires, as described in this section.

C. Intravalley acoustic phonon scattering

In this section, it is assumed that the phonon system remains in equilibrium and that the phonon wave functions can be approximated by their bulk counterparts.
Then, within the self-consistent Born approximation, the self-energy for the electron-phonon interaction is

$$\Sigma^< = D^< G^<, \tag{9}$$

with the free phonon lesser Green's function $D^<$ [3]. For the steady-state case, (9) can be written as

$$\Sigma^<(r, r', E) = \int \frac{dq}{(2\pi)^3} e^{iq(r-r')} |M_q|^2 \cdot \tag{10}$$
$$\left((N_q + 1) G^<(r, r', E + \hbar\omega_q) + N_q G^<(r, r', E - \hbar\omega_q)\right).$$

Assuming that $\hbar\omega_q \ll k_B T \Rightarrow E \pm \hbar\omega_q \approx E$, the phonon distribution function can be approximated by

$$N_q + 1 \approx N_q \approx \frac{k_B T}{\hbar\omega_q}, \tag{11}$$

and considering only intravalley acoustic phonons ($\hbar\omega_q = c_s q$), where the electron-phonon matrix element can be approximated by

$$|M_q|^2 \approx \frac{\hbar \Xi^2 q}{2\rho c_s}, \tag{12}$$

the term $|M_q|^2 \cdot N_q$ in (10) becomes independent of the phonon wave vector q, and therefore the self-energy becomes local in space:

$$\Sigma^<(r, r', E) = \frac{\Xi^2 k_B T}{\rho c_s^2} G^<(r, r', E) \delta(r - r'). \tag{13}$$

The mass density of silicon is $\rho = 2.329 g/cm^3$, the speed of sound in silicon is $c_s = 9.04 \cdot 10^5 cm/s$ and for the deformation potential we take $\Xi = 14.6 eV$ [8].
Once the lesser self-energy is given, the retarded self-energy can be calculated via

$$\Sigma^R(r, r', E) = \frac{1}{2}(\Sigma^>(r, r', E) - \Sigma^<(r, r', E)) + \tag{14}$$
$$iP \int \frac{dE'}{2\pi} \frac{\Sigma^>(r, r', E') - \Sigma^<(r, r', E')}{E - E'},$$

where $P \int dE'$ is the principal part of the integration. Since intravalley acoustic phonon scattering is treated as an elastic interaction here, (14) reduces to [5]

$$\Sigma^R(r, r', E) = \frac{\Xi^2 k_B T}{\rho c_s^2} G^R(r, r', E) \delta(r - r'). \tag{15}$$

Note that in the first line of (14) stands the anti-Hermitian part of $\Sigma^R(r, r', E)$, which is accountable for the dephasing. However, the quantum mechanical treatment of scattering also leads to a renormalization of the energies, which is represented by the Hermitian term in the second line of (14). It was claimed [7][8] that the Hermitian term can be neglected, since it leads to oscillations in the energy levels and therefore slows down the convergence, without introducing a significant error. In this work, we will analyze the influence of both terms on the electrostatic solution and the current.

D. Density and current calculation

For both the carrier density and the current, we basically have three contributions: coherent terms from the source/drain contacts (boundary terms) and an incoherent term from the acoustic phonon interaction.

$$G^< = G^R(\Sigma_S^< + \Sigma_D^< + \Sigma_{int}^<) G^A \tag{16}$$

$$n(x) = -i \sum_{v,\sigma} \sum_{nm} \int \frac{dE}{2\pi} G_{nm}^{<;v} \phi_n^v(x) \phi_m^v(x) \tag{17}$$

$$J_n(E) = -\frac{e}{\hbar} \sum_{v,\sigma} \sum_{l \geq n+1} \sum_{m \leq n} \int \frac{dE}{2\pi} \left(2Re(H_{lm}^v G_{ml}^{<;v})\right) \tag{18}$$

In (17) and (18) v and σ are the valley and spin indices.
As a consequence of density and current conservation in the device, the following important relation can be derived:

$$\sum_l \int \frac{dE}{2\pi} \left(2Re(H_{nl} G_{ln}^<)\right) = 0, \tag{19}$$

except at the boundaries to the source/drain contacts.
Equation (19) can be used as a physically motivated convergence criterion for the inner iteration loop of the self-energy and the Green's function, but only if we take the full retarded self-energy as in (15). Using only the first line of (14), current conservation is violated and (19) can not be used.

III. Simulation Procedure

A. General

The set of equations in Section II is completed with the inclusion of the Poisson equation. The basic simulation procedure is the following:

1) Solve the transverse Schrödinger equation (6).
2) Green's function - self-energy iteration: solve equations (8), (2), (13) and (15) until the convergence criteria are fulfilled (see Section III-B).
3) Calculate the density.
4) Compute new potential by solving the Poisson equation.
5) Iterate step 1) to 4) until convergence on the density and the potential is reached.

B. Convergence Criteria

Global convergence is achieved, when the self-consistent electrostatic solution fulfills a given error criterion. We apply the L^1 norm on the density and the L^∞ norm on the potential. Of special interest are the convergence criteria used for the inner iteration loop of the self-energy and the Green's function. In our simulations, we used the following criteria:

$$max(|\sum_l \int \frac{dE}{2\pi} \left(2Re(H_{nl}G^<_{ln})\right)|) < \epsilon_1 \cdot min(J_n) \quad (20)$$

$$max(|\Delta J_n|) < \epsilon_2 \cdot min(J_n) \quad (21)$$

$$\sum_i \int \frac{dE}{2\pi} |\Delta n(x_i)| < \epsilon_3 \cdot \sum_i \int \frac{dE}{2\pi} n(x_i). \quad (22)$$

Note again that (20) is only used if we consider (15).

C. Devices

We performed our simulations on two series of triple-gate silicon nanowires: The first has a quadratic cross-section of $3\,nm \times 3\,nm$ and the second of $5\,nm \times 5\,nm$ (Si only). Gate lengths from $5\,nm$ to $30\,nm$ were considered, taking $5\,nm$ steps, i.e. 6 different gate lengths in total.
Common to all our devices is that the source/drain extensions are $10\,nm$ long, thus the following holds for the device length L_d and the gate length L_g: $L_d = L_g + 20\,nm$.
The source/drain extensions are doped with an uniform arsenic concentration of $2e20\,cm^{-3}$, while the channel region has a very low boron concentration of $1e14\,cm^{-3}$.
An oxide layer of SiO_2 with a width of $0.6\,nm$ is wrapped around the silicon wire.
For the gate we used a workfunction of $4.1\,eV$.

D. Simulation modes

In order to investigate the effect of intravalley acoustic phonon scattering on the electrostatic solution and the current, we will compare the results of the following simulation modes in Section IV:

1) Ballistic simulation: $\Sigma^R_{int}(r,r',E) = \Sigma^<_{int}(r,r',E) = 0$
2) Full self-consistent acoustic phonon simulation: $\Sigma^R_{int}(r,r',E)$ is given by (15).
3) Semi self-consistent acoustic phonon simulation: $\Sigma^R_{int}(r,r',E)$ is given by the first line of (14), neglecting the Hermitian part.
4) Ballistic electrostatic solution, current calculation with acoustic phonons (15) as a post-processing step.
5) Ballistic electrostatic solution, current calculation with acoustic phonons (but only first line in (14)) as a post-processing step.

IV. Simulation Results

A. Drain-current vs gate-voltage

In Fig. 1 and Fig. 2 the I_D-V_g characteristics are shown for two different bias regimes $V_{SD} = 0.05V$ and $V_{SD} = 0.5V$ for the same device. For a better visualization of the difference between the various simulation modes, we show the ratios

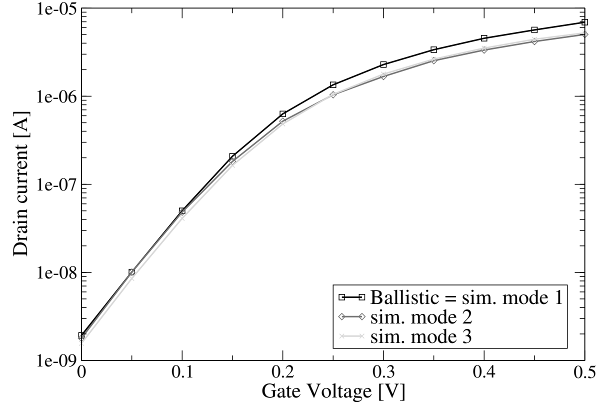

Fig. 1. Comparison of the I_D-V_g curves of the first three simulation modes with $V_{SD} = 50\,mV$, for a nanowire with a cross-section of $3\,nm \times 3\,nm$ and a gate length of $10\,nm$.

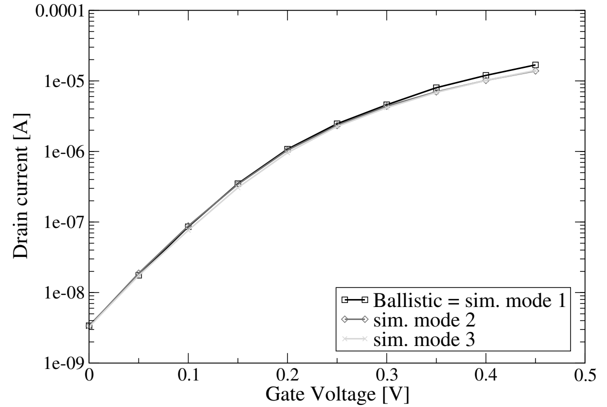

Fig. 2. Comparison of the I_D-V_g curves of the first three simulation modes with $V_{SD} = 500\,mV$, for a nanowire with a cross-section of $3\,nm \times 3\,nm$ and a gate length of $10\,nm$.

of the results in Fig. 3. The line with diamonds in Fig. 3 results only from the difference in the current calculation as a post-processing step to the same electrostatic solution, whereas the line with squares results from a different electrostatic solution and a difference in the current calculation. From Fig. 3 we learn that the error in the drain current, caused by the approximation in the third simulation mode compared to the second one, is up to $15\,\%$.

B. Subband profile

In Fig. 4 the shape of the lowest subband under the gate is shown. For all subbands in all other simulations, the situation is alike: simulation mode 2 has always the highest barrier, simulation mode 3 has the lowest barrier, i.e. lower than the ballistic case.

C. Scaling behavior

In *ballistic* simulations of nanodevices, the subtreshold current shows a strong dependence on the gate length due

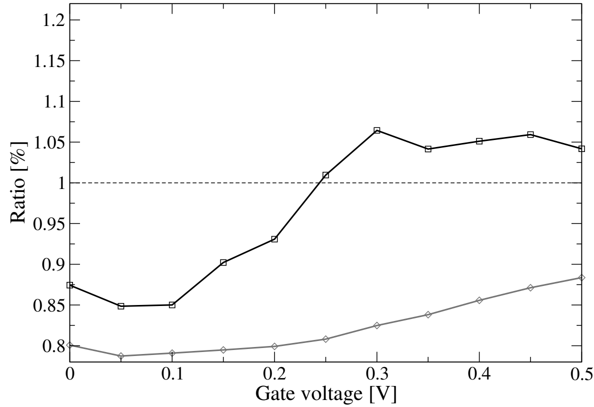

Fig. 3. For the same settings as in Fig. 1, the ratio between simulation mode 2 and 3 (squares) and between simulation mode 4 and 5 (diamonds) is shown.

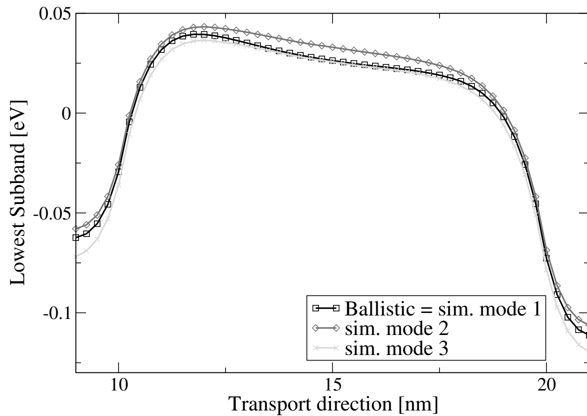

Fig. 4. For the same settings as in Fig. 1, the lowest subbands are shown for the first three simulation modes for $V_g = 0.25\,V$ and $V_{SD} = 50\,mV$.

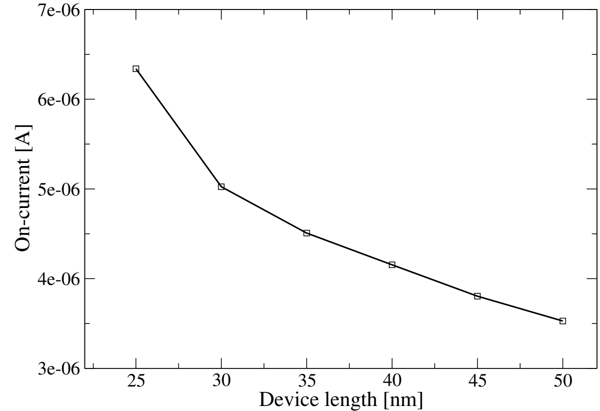

Fig. 5. Scaling of the nanowires with a cross-section of $3\,nm \times 3\,nm$ for $V_g = 0.5\,V$ and $V_{SD} = 50\,mV$ (simulation mode 2).

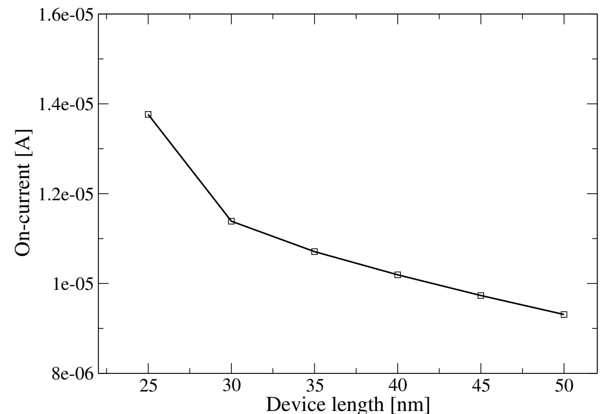

Fig. 6. Scaling of the nanowires with a cross-section of $5\,nm \times 5\,nm$ for $V_g = 0.5\,V$ and $V_{SD} = 50\,mV$ (simulation mode 2).

to tunneling currents. On the other hand, the on-current of the devices are almost independent of the gate length (and also of the device length), since once the barrier is gone, the transmission from source to drain is almost unity [9].
In simulations *with acoustic phonons*, the situation is completely different for the on-currents. As the device length increases, the coherent contribution (first two terms in (16)) to the density and the current decreases, whereas the incoherent term start to dominate. Then the on-current begins to scale linearly as a function of the device length, as shown in Fig. 5 and Fig. 6.

V. Conclusion

We have shown the scaling behavior of silicon nanowires in the presence of intravalley acoustic phonon scattering and presented a quantitative analysis of the error in the drain current caused by the negelection of the Hermitian term in the retarded self-energy, which is up to $15\,\%$ of the current.

Acknowledgment

The authors would like to thank Prof. W. Fichtner, Dr. M. Luisier and S. Steiger for interesting discussions and hints. This work had financial support by the Swiss National Science Foundation (project NEQUATTRO SNF 200021-109393/1) and the European project PULLNANO (IST-4-026828).

References

[1] L. V. Keldysh, Sov. Phys. JETP 20, 1018 (1965)

[2] L. P. Kadanoff and G. Baym, *Quantum statistical mechanics* (Benjamin, New York, 1962)

[3] G. D. Mahan, *Many-particle physics* (Kluwer Academic / Plenum Publishers, New York, 2000)

[4] S. Datta, *Electronic transport in mesoscopic systems* (Cambridge University Press, New York, 1995)

[5] R. Lake, G. Klimeck, R. C. Bowen and D. Jovanovic, Journal of Applied Physics 81, 7845, 1997

[6] R. Venugopal, Z. Ren, D. Jovanovic, S. Datta and M. Lundstrom, Journal of Applied Physics 92, 3730, 2002

[7] A. Svizhenko and M. P. Anatram, IEEE Trans. Electron Devices 50, 1459, 2003

[8] S. Jin, Y. Park and H. S. Min, Journal of Applied Physics 99, 123719, 2006

[9] F. O. Heinz and A. Schenk, Journal of Applied Physics 100, 084314, 2006